PAPER • OPEN ACCESS

Influence of heat treatment on the microstructure and surface groups of Stöber silica

To cite this article: Shanshan Li *et al* 2023 *Mater. Res. Express* **10** 105004

Materials Research Express

PAPER

Influence of heat treatment on the microstructure and surface groups of Stöber silica

Shanshan Li[1], Shuguang Yang[2,3], Shu Xu[1] and Quan Wan[2,*]

[1] School of Chemistry and Materials Science, Guizhou Normal University, Guiyang 550025, Guizhou, People's Republic of China
[2] State Key Laboratory of Ore Deposit Geochemistry, Institute of Geochemistry, Chinese Academy of Sciences, Guiyang 550081, Guizhou, People's Republic of China
[3] University of Chinese Academy of Sciences, Beijing 100049, People's Republic of China
[*] Author to whom any correspondence should be addressed.

E-mail: wanquan@vip.gyig.ac.cn

Keywords: Stöber silica, heat treatment, microstructure, surface groups

OPEN ACCESS

RECEIVED
13 July 2023

REVISED
22 September 2023

ACCEPTED FOR PUBLICATION
2 October 2023

PUBLISHED
12 October 2023

Abstract

Heat treatment is routinely utilized in preparing nanoporous materials (including Stöber silica), and can substantially affect their performance in diverse application fields. However, the effects of heat treatment at different temperatures on the structure and surface properties of Stöber silica have not been systematically investigated before. In this work, Stöber silica (washed with water or ethanol) was calcined at different temperatures (from 250 °C to 1000 °C), and the heat-treated samples were characterized through nitrogen adsorption at 77 K, scanning electron microscopy, simultaneous thermal analysis, elemental analysis, and Fourier-transform infrared spectroscopy. The results show that there is no significant difference in the morphology and particle size of the calcined samples. The internal micropores almost collapse after calcination at 500 °C, and the pores with a smaller diameter are the first to shrink during calcination. The variation in the number of the surface hydroxyl groups and ethoxyl groups with the calcination temperature is discussed in detail. The carbon content analysis and differential scanning calorimetry curves reveal that the surface ethoxyl groups (for the samples washed with ethanol) are completely removed after calcination at 500 °C. After calcination at temperatures above 800 °C, the hydroxyl groups almost completely condense into siloxanes. The specific surface area calculated according to the thermogravimetric mass loss and surface hydroxyl density is found to be significantly different from the measured Brunauer–Emmett–Teller specific surface area. Our results may offer practical guidance for the application of Stöber silica subjected to similar heat-treatment processes.

1. Introduction

Nanoporous silica has received considerable research interest due to its unique characteristics, such as adjustable pore size, high specific surface area, large pore volume, controllable morphology, and flexible surface modification, and it has been studied for application to various fields, such as biomedicine [1], catalysis [2], adsorption [3], storage [4], and optics [5]. Stöber silica is one of the most popular nanoporous silica materials due to its monodispersed spherical morphology and simple synthesis process. It can be used in a broad range of fields, such as photonic crystals [6], core–shell composite particles [7], dental filler materials [8], and catalyst supports [9]. In these fields, the simple synthesis route, porous structure, numerous surface groups, and regular spheres of Stöber silica play an important role. For example, the pore size of the silica shell influences the mass transport properties of Au@SiO_2 nanorods, and the simple synthesis route of Stöber silica has been adopted to fabricate a nonporous (or ultramicroporous) silica shell [10]. The regular spherical particles of Stöber silica have been utilized to prepare photonic crystals, and the moisture and organic by-products of the micropores inside and on the surface of Stöber silica have been found to affect the quality of the fabricated photonic crystals [6]. Post-synthesis treatments influence the microporous structure of Stöber silica. Using Stöber silica after being

subjected to an appropriate post-synthesis treatment as a support, a highly dispersed Ni^{2+} catalyst has been prepared by impregnating Ni^{2+} ions into the micropores [9].

Heating is a common treatment method adopted either before or during the application of silica in order to achieve specific properties or conditions. For example, Stöber silica was heat treated to remove impurities as well as adsorbed and structural water for fabricating high-quality photonic crystals [6]. Heat-treated silica has been reported to exhibit a significant ability to trap O_2 molecules because a thick region is generated during heating and the molecules can occupy the silica matrix interstices [11]. A heat treatment has been utilized to control the silanol density on the silica surface for investigating the proton conductivity of polymer-coated silica [12]. The structural changes of mesoporous silica with the heating temperature were studied, and the thermal conductivity was found to be related to the microstructure [13]. As widely recognized, heat treatment can alter the surface groups and pore structure of silica. Therefore, it is reasonable to assume that heat treatment will also modify the surface and internal structures of Stöber silica, thus affecting its performance in various applications.

Since the Stöber synthesis process was first reported in 1968 [14], the particle size variation with the synthesis conditions [15, 16], particle nucleation and growth theory [17, 18], and modification of the synthesis method [19–21] have been systematically investigated by many research groups. The influence of heat treatment on the variation in the internal micropore structure and surface groups of Stöber silica has been noticed for a long time. For example, Motoyoshi *et al* demonstrated the influence of heat treatment on the charging behavior of Stöber-type silica and discussed its colloidal stability [22]. Romeis *et al* reported the mechanical properties of Stöber silica treated at different heating temperatures, which were found to be related to the internal structure [23]. Moreover, the densification behavior, evolution of the microstructure, and sintering of Stöber silica were investigated [24]. Furthermore, the variation in the number of the surface hydroxyl groups with the reaction conditions was studied, and the density of the surface hydroxyl groups was calculated [25]. However, up to now, systematic studies on the variation in the internal micropore structure and surface groups of Stöber silica with heat treatment have been limited. There is still a current need to subject Stöber silica to different heat treatment processes and investigate the changes in its internal and surface properties. The complex internal pore structure of Stöber silica is thought to be one of the main obstacles to investigating the variation in the microporous structure and surface groups with the heat treatment. For example, pycnometry, acid–base titration, liquid-phase adsorption, and small-angle x-ray scattering results indicated that Stöber silica exhibits a microporous structure [26–31]. However, the Brunauer–Emmett–Teller (BET) specific surface area (S_{BET}) derived from nitrogen adsorption measurements at 77 K (which is the conventional measurement method for porous materials) was found to vary over a wide range of values (from several m^2/g to several hundred m^2/g) [32–35]. These discrepant results led to a confused understanding of the Stöber silica microstructure and prevented its application.

In the previous experimental works [36, 37], it was found that the reaction time, washing solvents used, and drying conditions influence the S_{BET} of Stöber silica as measured via N_2 adsorption at 77 K. In these previous works, Stöber silica was synthesized with an S_{BET} ranging from about 11 to 360 $m^2\ g^{-1}$, and the sample with a large S_{BET} was found to possess a microporous structure with a 0.8 nm pore diameter. Suitable synthesis conditions were identified, including a short reaction time, washing with water, and drying at a low temperature without the need of vacuum. The pore-blocking mechanism involving silica monomers or oligomers, ethoxyl groups, and the condensation reactions of silanol or ethoxyl groups were also discussed. In the previous works, the relationships between the internal micropore structure, S_{BET} values of Stöber silica, and post-treatment processes were understood, which provide a foundation for the systematic studies in this paper.

To investigate the influence of heat treatment temperature on the microstructure and surface groups of Stöber silica, in this study, Stöber silica was fabricated and washed with water or ethanol, which are two conventional washing solvents, and were found to significantly influence the microporous structure of Stöber silica [36, 37]. After drying, the samples were calcined at different temperatures (from 250 °C to 1000 °C). Then, the samples were characterized by N_2 adsorption, attenuated total reflection infrared spectroscopy (ATR-IR) , simultaneous thermal analysis (STA), scanning electron microscopy (SEM) and elemental analysis, through which, the variation in the particle morphology, internal pore structure, and number of surface silanol and ethoxyl groups with the heating temperature was investigated. The research findings suggest that pores of smaller size are more susceptible to shrinkage or collapse during the heat treatment process, and all micropores in the samples disappear when the calcination temperature exceeds 500 °C. It is also implied that the hydroxyl and ethoxyl groups of the samples can be regularly controlled via varying heating temperature.Our work reveals the evolution of pore structure and surface groups of Stöber silica during heating, and may therefore provide practical guidance on the heat-treatment process of Stöber silica in order to promote its applications in various fields such as composite materials, catalysis, optics, and storage.

2. Materials and methods

2.1. Materials

Tetraethoxysilane (TEOS, purity > 99%) and ammonia (purity: 25%–28%) were purchased from Aladdin (Shanghai, China) and used without further treatment. Ethanol (purity > 99.7%) was supplied by Sinopharm Chemical Reagent, China. Deionized water was obtained from a Millipore system and had a resistivity of 18.2 MΩ·cm.

2.2. Synthesis of Stöber silica

For the synthesis, 8.5 mL of ammonia, 26.3 ml of deionized water, and 191.2 mL of ethanol were mixed in a flask and stirred at 20 °C. Additionally, 20 ml of TEOS and 2 ml of ethanol were mixed and stirred in the same conditions. After 45 min, 14 ml of the TEOS and ethanol mixture was added to the ammonia, deionized water, and ethanol mixture, and the obtained mixture was continuously stirred for 80 min. After reacting, the suspension was centrifuged at 10,000 rpm (9940 g) to collect the precipitate of the silica particles.

2.3. Treatment of the synthesized products

The collected silica product was divided into two parts; one was washed with deionized water and the other one was washed with ethanol (because deionized water and ethanol are the two most commonly used washing solvents for synthesizing Stöber silica). Each washing procedure was performed using a vortex mixer for 2 min with 30 ml of the washing solvent; then, the suspension was centrifuged and separated. After being washed four times, the samples were first dried at 50 °C for 2 h and then dried at 200 °C for 2 h (the samples were placed in an oven at the target temperature), which is an effective method to obtain microporous Stöber silica according to the previous work [37]. The samples washed with deionized water and ethanol are denoted as W-200 and E-200, respectively. Then, samples W-200 and E-200 were calcined at 250 °C, 300 °C, 400 °C, 500 °C, 600 °C, 800 °C, or 1000 °C for 4 h. The resulting samples are denoted as W-250 (E-250), W-300 (E-300), W-400 (E-400), W-500 (E-500), W-600 (E-600), W-800 (E-800), and W-1000 (E-1000), respectively. The calcination process was conducted via thermogravimetry (TG), and each sample was heated in a dry atmosphere at a heating rate of 2 °C min^{-1}.

2.4. Characterization of the synthesized samples

Scanning electron microscopy (SEM, Scios, FEI Company, USA) imaging was conducted to investigate the morphology of the samples. Nitrogen adsorption (77 K) was performed using an Automated gas sorption analyzer (Autosorb-iQ, Quantachrome, USA), and the samples were outgassed for 12 h at 200 °C prior to the measurements. The nonlocal density functional theory (NLDFT) and multi-point BET method were employed to analyze the pore size, pore volume, and specific surface area. The thermal properties of the samples were characterized using a simultaneous thermal analyzer capable of performing TG and differential scanning calorimetry (DSC) (STA 449F3, Netzsch, Germany). During the measurements, each sample (15–25 mg) was heated from 50 °C to 1200 °C in a dry air atmosphere at a heating rate of 10 °C min^{-1}. The Fourier-transform infrared (FTIR) spectra were acquired via attenuated total reflectance (ATR)-FTIR spectroscopy (Vertex 70, Bruker, Germany). The spectral range was from 4000 to 400 cm^{-1}, the resolution was 4 cm^{-1}. The carbon content of each sample (30–50 mg) was determined using an elemental analysis instrument (Vario MACRO cube, Elementar, Germany).

3. Results and discussion

3.1. Characterization of the Stöber silica particles

The SEM micrographs of samples W-200, E-200, W-600, and W-1000 are presented in figure 1. Samples W-200 and E-200 were washed with water and ethanol respectively, and the samples W-600 and W-1000 were obtained by calcining the sample W-200 at 600 °C and 1000 °C respectively.

As shown in figure 1, the spherical particle morphology was not significantly influenced by the washing solvents or heat treatment. The average diameter of the particles, which was measured using the ImageJ software, is about 350 nm. Although differences of a few nanometers in the average diameter between samples may exist, we believe such minor discrepancies are mainly due to measurement errors and consider them negligible for particles with a size of 350 nm. In other words, under our experimental conditions, neither the washing solvents nor the heating temperatures seem to have a discernible impact on particle size. Although some previous studies demonstrated that Stöber or Stöber-type samples might shrink by 6%–8% when calcinated at temperatures above 800 °C [22, 23], this generally required calcination durations (12 h or 24 h) much longer than that (4 h) in

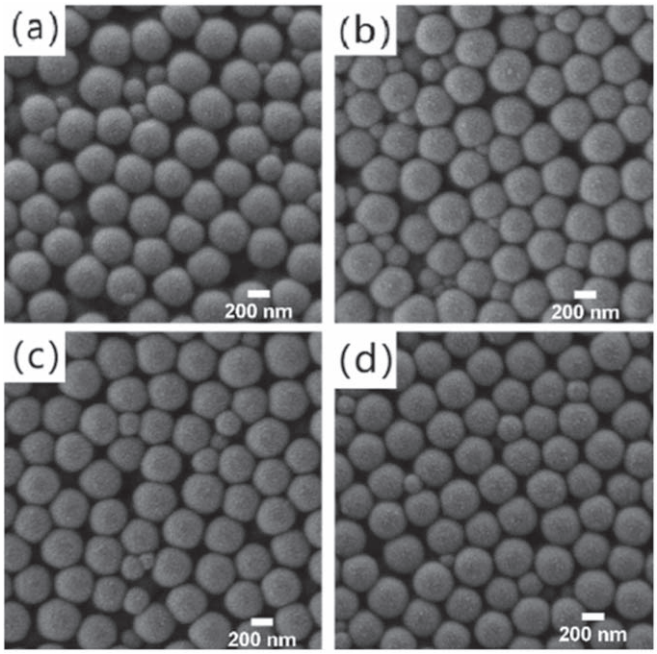

Figure 1. SEM images of representative samples. (a) Sample W-200; (b) sample E-200; (c) sample W-600; and (d) sample W-1000.

our work. Apparently, the duration of calcination plays an important role affecting the sample's structural characteristics, which may deserve further investigation in the future.

The N_2 adsorption isotherms of the Stöber silica samples that were washed with water and ethanol (samples W-200 and E-200) are shown in figure 2(a). According to the IUPAC classification, the isotherm of sample W-200 is classified as a type I isotherm [38]. The initial adsorption amount of N_2 in a Type I isotherm increases sharply, indicating the presence of narrow micropores within the sample. The pore size distribution of sample W-200 obtained from the NLDFT model (figure 2(c)) shows that the main pore widths are ~0.8 nm and ~1.1 nm, which is consistent with the type I isotherm. The measurement time was 55 h, and the sample mass was 65.8 mg, which are normal measurement conditions for microporous samples. At low relative pressures, the desorption and adsorption branches of sample W-200 do not meet, indicating that the micropores are small or have a complex shape or channel, so that the desorption/adsorption equilibrium cannot easily be reached within a short time [39]. The isotherm of sample E-200 is classified as a type II isotherm, indicating a nonporous structure [38]. The S_{BET} values of samples W-200 and E-200 are 343.5 and 18.0 $m^2\ g^{-1}$, respectively. As reported in the previous works [36, 37], deionized water can remove the monomers or oligomers and ethoxyl groups that block the pore channels, while ethanol converts the surface silanol groups into ethoxyl groups and further blocks the pore entrances or channels. Therefore, despite the same synthesis conditions with except of the washing solvent, the N_2 adsorption curves are very different.

3.2. Influence of the heat treatment on the microstructure

Similar to that of sample W-200, the isotherms of samples W-250 and W-300 can also be classified as type I isotherms (figure 2(b)) but the amount of the adsorbed nitrogen molecules in the initial stage is reduced. In contrast to sample W-200, the decrease in the adsorption amount suggests a reduction in the volume of the micropores within the samples W-250 and W-300, which is consistent with the pore size distribution shown in figure 2(c) and the specific surface areas presented in Table 1. It can be observed from figure 2(c) that after calcination at 250 °C, the peak corresponding to the pore size of 0.8 nm decreases to the height similar to that of 1.1 nm. Subsequently, after calcination at 300 °C, the peak for the 0.8 nm pores continues to decrease below that of the 1.1 nm, indicating a significant reduction in the volume of pores with a size of 0.8 nm during the calcination process. On the other hand, with the temperature increased from 200 to 300 °C, there is also a decrease observed in the peak for pores with a size of 1.1 nm. However, the decrease in the peak height value (from 0.15 to 0.13 $cm^3\ nm^{-1}\ g^{-1}$) for the 1.1 nm pores is much smaller than that (from 0.3 to 0.1 $cm^3\ nm^{-1}\ g^{-1}$) for the 0.8 nm pores. This observation suggests that the smaller-sized pores are more susceptible to shrinkage or collapse during calcination, resulting in a drastic reduction of nitrogen molecules entering the narrower pores during the gas adsorption measurement. Table 1 shows that the specific surface area of sample W-200 decreased from 343.5 to 311.0 $m^2\ g^{-1}$ after calcination at 250 °C, and further decreased to 246.0 $m^2\ g^{-1}$ after calcination at

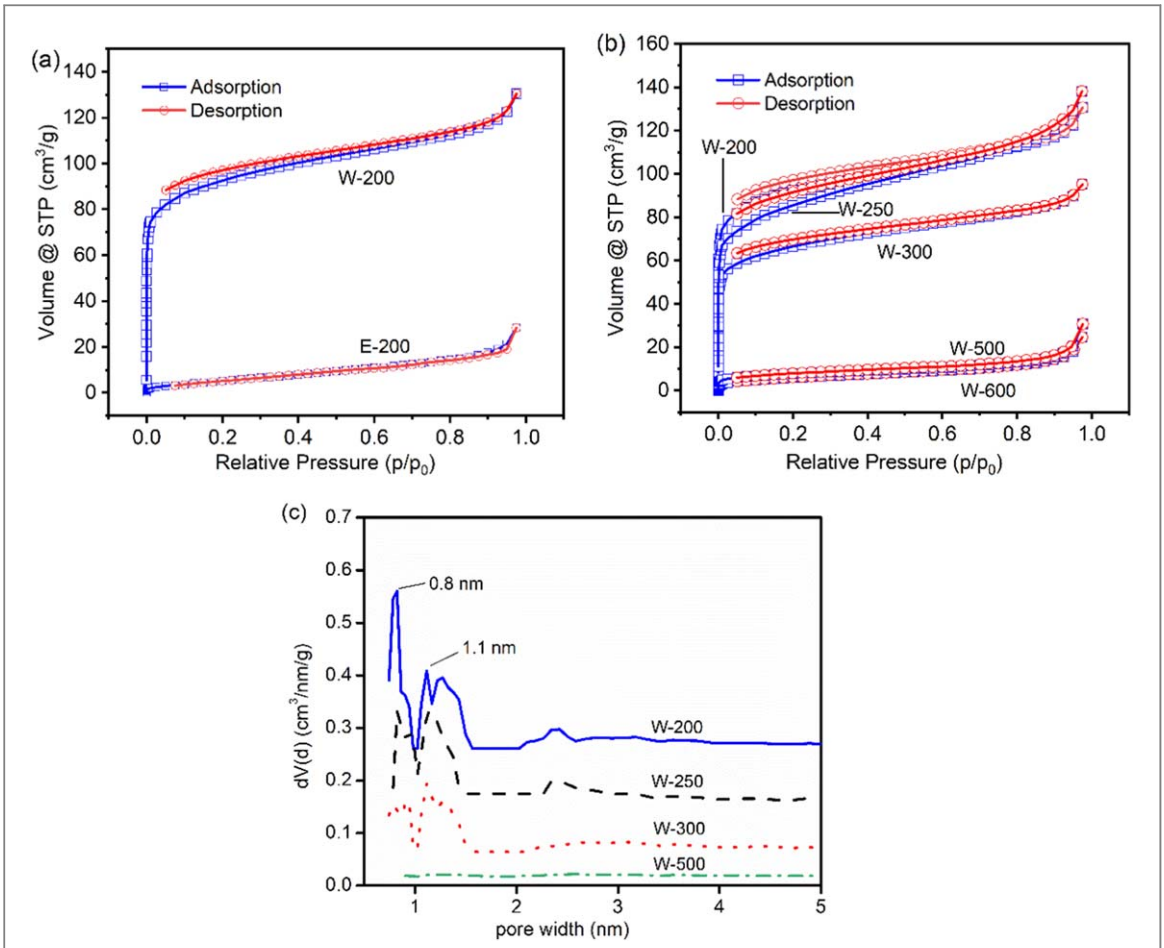

Figure 2. N_2 adsorption isotherms at 77 K and pore size distribution of representative samples. (a) N_2 adsorption isotherms of samples W-200 and E-200; (b) N_2 adsorption isotherms of samples W-200, W-250, W-300, W-500, and W-600; (**c**) pore size distribution of samples W-200, W-250, W-300, and W-500 obtained from the NLDFT.

Table 1. Analysis results of the gas adsorption measurements for the samples washed with water.

Sample	$S_{BET}(m^2/g)$	Pore width (nm)	Pore volume (cc/g)	Micropore volume (cc/g)
W-200	343.5	0.8	0.20	0.1
W-250	311.0	0.8/1.1	0.19	0.08
W-300	246.0	1.1	0.14	0.07
W-500	27.8	2.6	0.05	—
W-600	22.0	3.2	0.04	—
W-800	20.9	3.8	0.04	—
W-1000	18.9	4.9	0.04	—

300 °C.The micropore volume of the samples (table 1) decreases from 0.1 cc g^{-1} to 0.08 cc g^{-1} after calcination at 250 °C, and further diminishes to 0.07 cc g^{-1} after calcination at 300 °C. The pore volume of the samples also exhibits a similar trend. These declining specific surface areas, micropore volume, etc, with increasing calcination temperature, are indicative of pore shrinkage or collapse during the calcination process.The divergence of the desorption and adsorption branches is also apparent in the isotherm of samples W-250 and W-300, and it can also be attributed to the small pores. The N_2 adsorption measurement for sample W-400 did not finish because it was too slow. After 90 h of measurement, the relative pressure reached only 5.2×10^{-3}. This means that the temperature of 400 °C causes the micropores to shrink or be blocked further, so that the nitrogen molecules are hindered from entering or diffusing into the micropores. However, the amount of 47 cc g^{-1} of the adsorbed nitrogen molecules indicates a considerable S_{BET} (the amount of the adsorbed molecules for sample W-300 at the same relative pressure is about 51 cc g^{-1}), which suggests the existence of a large number of internal

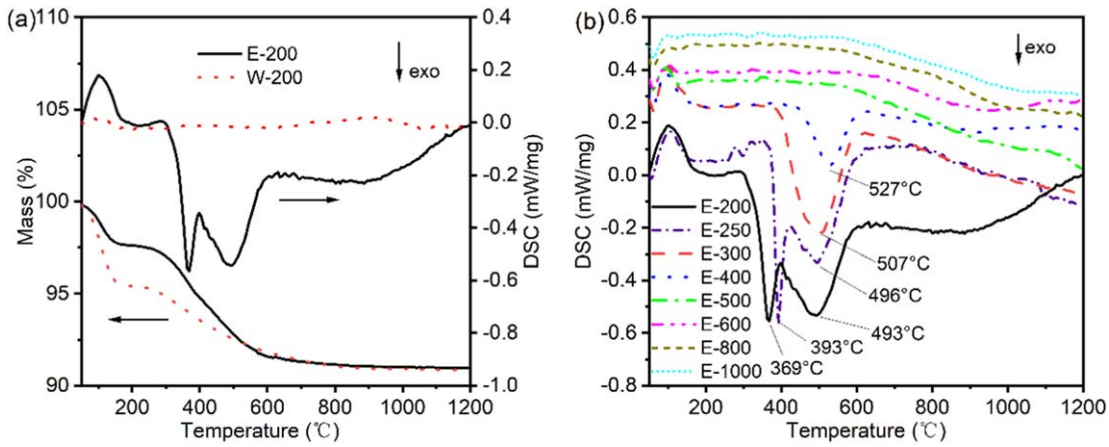

Figure 3. (a) TG and DSC curves of samples W-200 and E-200; (b) DSC curves of the samples washed with ethanol.

Table 2. Specific surface area calculated using the BET model and carbon content of the samples washed with ethanol.

Sample	E-200	E-250	E-300	E-400	E-500	E-600	E-800	E-1000
S_{BET} (m^2/g)	18.0	21.6	19.9	14.2	21.2	17.8	16.9	19.9
Carbon content (%)	1.50	1.45	1.30	0.47	0.06	—	—	—

micropores. After calcination at 500 °C, the micropores almost collapse, or their entrance is blocked, so the isotherm is consistent with a type II isotherm, and the S_{BET} drops dramatically to 27.8 $m^2\ g^{-1}$. The isotherm of sample W-600 is very close to that of sample W-500, and the S_{BET} decreases to 22.0 $m^2\ g^{-1}$; additionally, the pore volume also decreases from 0.05 to 0.04 cc g^{-1}. The isotherms of the samples calcined at higher temperatures almost overlap with that of sample W-600; this is why the isotherms of samples W-800 and W-1000 are not shown in the figure. Above 500 °C, the temperature has little effect on the S_{BET} because the micropores are already destroyed. The pore width in table 1 gradually increases with the calcination temperature, which also illustrates that smaller pores shrink or are blocked more easily than larger ones.

The isotherms of the samples washed with ethanol almost overlap with that of sample E-200. The S_{BET} values of the ethanol-washed samples are summarized in table 2. Table 2 shows that the S_{BET} values of all samples are similar and indicate a nonporous structure, which demonstrates that the blocked pore channels could not be cleared during the heat treatment. Despite the fact that the ethoxyl groups are burned and removed during the heat treatment (as will be discussed in section 3.3), the monomers or oligomers, the condensation of the silanol groups, and the simultaneous shrinkage of the micropores are the main contributors to the blocking of the pores.

3.3. Influence of the heat treatment on the surface properties

The TG and DSC curves of samples W-200 and E-200 are presented in figure 3(a). The mass loss below 200 °C indicates the removal of the physically adsorbed water. The mass loss above 200 °C results from the removal of the surface hydroxyl or ethoxyl groups, which accompany an endothermic process or an exothermic process, respectively [40]. In figure 3(a), a clear difference in the DSC curves above 200 °C is observed (see the two exothermic peaks for sample E-200). During synthesis, the ethoxyl groups originated from the incomplete hydrolyzed TEOS (Si–OC_2H_5) remain on the particle surface after reaction. When the sample is washed with water, the residual ethoxyl groups on the surface are almost hydrolyzed (the carbon content of sample W-200 is negligible); by contrast, when the sample is washed with ethanol, a proportion of the hydroxyl groups on the surface is converted into ethoxyl groups [37]. Thus, the exothermic peaks at 369 °C and 493 °C for sample E-200 represent the oxidation of the ethoxyl groups in air. After calcination at 250 °C, the exothermic peak of 369 °C shifted to 393 °C, while the peak of 493 °C shifted to 496 °C. However, for sample E-300 (figure 3(b)), the exothermic peak at 369 °C disappears, while the exothermic peak at 507 °C remains visible on the DSC curve.

In the previous works [36, 37], it was found that after the monomer concentration caused by the TEOS hydrolysis reaches a critical supersaturation level, a quick burst of the nucleation process takes place. Then, the nuclei aggregate and form interparticle pores, and the subsequent addition of monomers or oligomers may block the pore channels; the extent of clogging might become severe after ethanol washing. The burning of the

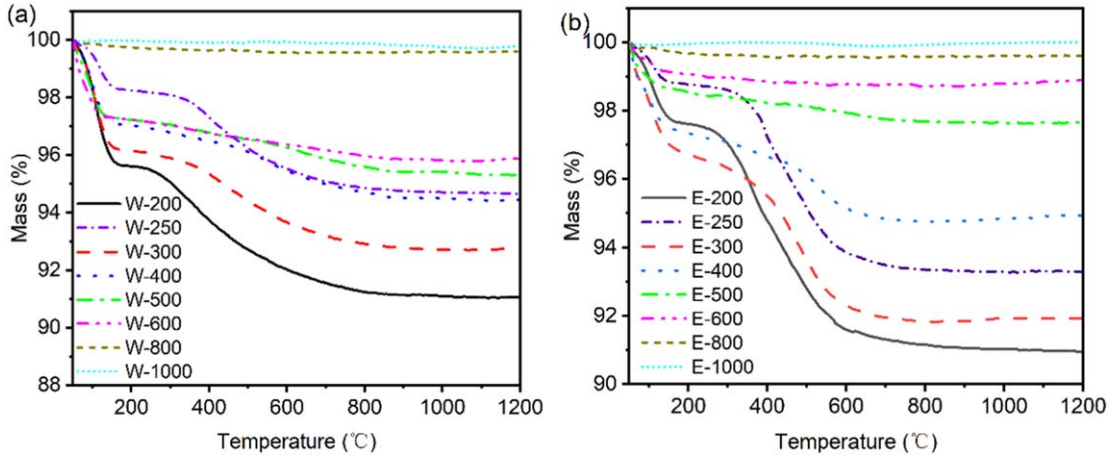

Figure 4. TG curves of the samples washed with (a) water and (b) ethanol.

Table 3. TG mass loss from 200 °C to 1200 °C for all samples.

Sample	Mass loss (%)	Sample	Mass loss (%)
W-200	4.54	E-200	6.66
W-250	3.59	E-250	5.47
W-300	3.38	E-300	4.63
W-400	2.58	E-400	2.24
W-500	1.92	E-500	0.87
W-600	1.36	E-600	0.17
W-800	0.20	E-800	0.08
W-1000	0.11	E-1000	0.05

ethoxyl groups located at different sites may require different temperatures [40]. According to the discussion in section 3.2, after calcination at 250 °C, some ethoxy groups were removed and the micropores also shrunk. Because of the shrinkage of micropores, a higher temperature may be required for the remaining ethoxy groups inside the micropores to be released, and thus the exothermic peak shifts towards higher temperatures. Similarly, after calcination at 300 °C, the disappearance of the peak at 393 °C suggests that perhaps the ethoxy groups inside the smaller micropores have been almost completely removed, which is in line with the continued reduction in the peak at 0.8 nm pores in figure 2(c). In the DSC curve of sample E-400, the exothermic peak caused by the residual ethoxyl groups shifts to 527 °C (see figure 3(b)). The gradually increasing temperature of the exothermic peak means that it becomes more difficult to remove the residual ethoxyl groups in the interior after calcination. The gradually decreased carbon contents in the samples (derived from Si–OC_2H_5), which are presented in table 2, correspond to the gradually weakened exothermic peaks (for samples E-200, E-250, E-300, and E-400). The ethoxyl groups are almost removed during calcination at 500 °C, as can be inferred from the DSC curve of sample E-500. The 0.06% carbon content is consistent with the fact that the exothermic peak has disappeared. Furthermore, the DSC curves of samples E-600, E-800, and E-1000 exhibit little difference with respect to that of sample E-500 due to the complete removal of the ethoxyl groups. The negligible carbon contents in these samples also confirm the occurrence of the exothermic process caused by the ethoxyl groups. The DSC curve of sample W-200 has no clear peak above 200 °C due to the weak endothermic process of deprive of the surface hydroxyl group in a wide temperature range (from 200 °C to 1200 °C) and the small number of ethoxyl groups (the carbon content of sample W-200 is less than 0.06%). The DSC curves of the calcined water-washed samples are not depicted in the figure as they are similar to that of sample W-200.

The TG curves of all samples are shown in figure 4, and the mass losses at a temperature above 200 °C are summarized in table 3. The higher TG mass loss of sample E-200 (6.66%) with respect to that of sample W-200 (4.54%) (see table 3) above 200 °C demonstrates the occurrence of a strong exothermic process because the weight loss of the ethoxyl groups is much higher than of the hydroxyl groups. For amorphous silica, after calcination at 400 °C, the concentration of the surface hydroxyl groups (2.35 OH nm^{-2}) is considered about half of that of the sample dried at 200 °C (4.6 OH nm^{-2}) [41]. This indicates that the surface hydroxyl groups of the samples washed with water are gradually removed during heating, and the mass loss above 200 °C decreases

from 4.54% (for sample W-200) to 2.58% (for sample W-400). However, for the samples washed with ethanol, there is a considerable number of ethoxyl groups on the surface, most of which can be removed upon calcination at 400 °C (the exothermic peak area of sample E-200 (530.3 J g^{-1}) is nearly five times that of sample E-400 (108.6 J g^{-1})). The mass loss above 200 °C decreases drastically from 6.66% (for sample E-200) to 2.24% (for sample E-400), which is consistent with the carbon contents listed in table 2. Therefore, only a few ethoxyl groups and a certain number of hydroxyl groups remain on the surface of sample E-400, so the mass loss above 200 °C (2.24%) is lower than that of sample W-400 (2.58%). This means that after washing with ethanol, most surface sites are occupied by the ethoxyl groups. At the same trend, after calcination of the ethoxyl groups, the few residual hydroxyl groups result in a lower mass loss for the ethanol-washed samples compared with that of the water-washed samples. For example, the mass loss of sample E-500 is 0.87%, and the mass loss of sample W-500 is 1.92%. Similarly, the mass loss of sample E-600 (0.17%) is much smaller than that of sample W-600 (1.36%). From table 2 and figure 3(b), it can be seen that after calcination at 500 °C, the ethoxyl groups are completely removed, which is in agreement with the collapse of the internal micropores that was inferred from the gas adsorption measurements. From tables 1 and 3, it can be seen that the specific surface area of the water washed sample decreases to 22.0 m^2 g^{-1} after calcination at 600 °C, while its hydroxyl mass loss (from 200 °C to 1000 °C) obtained from TG analysis is 1.36%. According to the calculation based on a surface hydroxyl density of 4.6 OH/nm^2 (as described in section 3.4), the hydroxyl mass loss on a surface area of 22.0 m^2 g^{-1} should be less than 0.2%. This also indicates that the mass loss is not only caused by hydroxyl groups on the outer surface but mainly due to those on the inner surface. Although nitrogen adsorption measurements show a nearly complete reduction of pores for sample W-600, such a result takes into account only the pores that can be accessed by nitrogen molecules. It is highly likely that there exist inside the sample smaller-sized or even closed pores inaccessible to nitrogen molecules, but their surface hydroxyl groups will still condense into siloxane (Si–O–Si) during TG measurement. From figure 4(a), it can be observed that the TG curve for sample W-600 shows a significant weight loss before reaching 800 °C and then becomes relatively flat afterward. The TG curves of samples after calcination at 800 °C and 1000 °C exhibit a tendency to plateau in figure 4 with small mass losses (<0.2%). This suggests that when calcination temperature exceeds 800 °C, hydroxyl groups inside the sample have essentially condensed into siloxane, resulting in the complete disappearance of internal pore structure, which is also consistent with the previous research [23, 29]. There have been some applications of Stöber silica after high temperatures treatment. For example, a nonporous sample was produced at high temperatures (900 °C–1000 °C) [11]; the surface charges were studied after calcination at 800 °C [22]; the effects of heat treatment at 700 °C on material thermal conductivity and structural changes were investigated [13]; the pores and surface properties were researched after calcination at 800 °C [29], etc. Therefore, investigation of heat treatment at a temperature as high as 1000 °C not only facilitates a better comprehension of the structural evolution, but also provides a reference for relevant applications.

The ATR-FTIR spectra also illustrate the same variation trend of the number of surface groups. The absorption peaks at 449, 800, and 1068 cm^{-1} are attributed to the rocking of the oxygen atoms in the SiO_2 structure, the bending motion of the Si–O–Si bridges, and the asymmetric stretching vibration of the Si–O–Si bridges, respectively (see figure 5(a)) [42], which do not significantly change during calcination. The peak at 942 cm^{-1} is assigned to the stretching vibration of the Si–OH groups [42], which gradually diminishes with increasing calcination temperature and almost disappears at a calcination temperature of 500 °C (figure 5(b), (c)). The curves of samples E-300 and E-400 displayed in figure 5(d) exhibit lower absorbance at 942 cm^{-1} than those of samples W-300 and W-400, which indicates the smaller number of hydroxyl groups in the ethanol-washed samples than in the water-washed samples, as mentioned above. The absorption peak at 2983 cm^{-1} is attributed to the stretching vibration of the C–H bonds in the ethoxyl groups [42]. As mentioned above, for the samples washed with water, the residual ethoxyl groups on the surface are converted into hydroxyl groups during washing, so the FTIR curves do not show any pronounced absorption at 2983 cm^{-1}. However, a distinct absorption peak at 2983 cm^{-1} is observed for sample E-200 (figure 5(a)), the intensity of which also decreases with increasing calcination temperature (figure 6(a)). For sample E-500, the absorption peak at 2983 cm^{-1} disappears completely, which is consistent with the carbon content and the results of the DSC measurements. The broadband region from 3200 to 3700 cm^{-1} corresponds to different O–H stretching modes in SiO–H and H_2O [43]. With increasing calcination temperature, the surface silanol is gradually removed. By comparing figures 6(a) and 6(b), it can be observed that the curves of the samples washed with water show stronger absorption in this broadband region than the samples washed with ethanol for the same calcination temperature, which also confirms the smaller number of hydroxyl groups in the samples washed with ethanol. In the range of 3200–3700 cm^{-1}, there is a distinctive absorption peak at about 3668 cm^{-1}, which is assigned to internal silanol [44]. The peak at 3668 cm^{-1} shifts toward a higher wavenumber with increasing calcination temperature, which has been reported to be due to the heterogeneity of the internal silanols, and the absorption at a lower wavenumber was found to be the first to disappear during calcination [44].

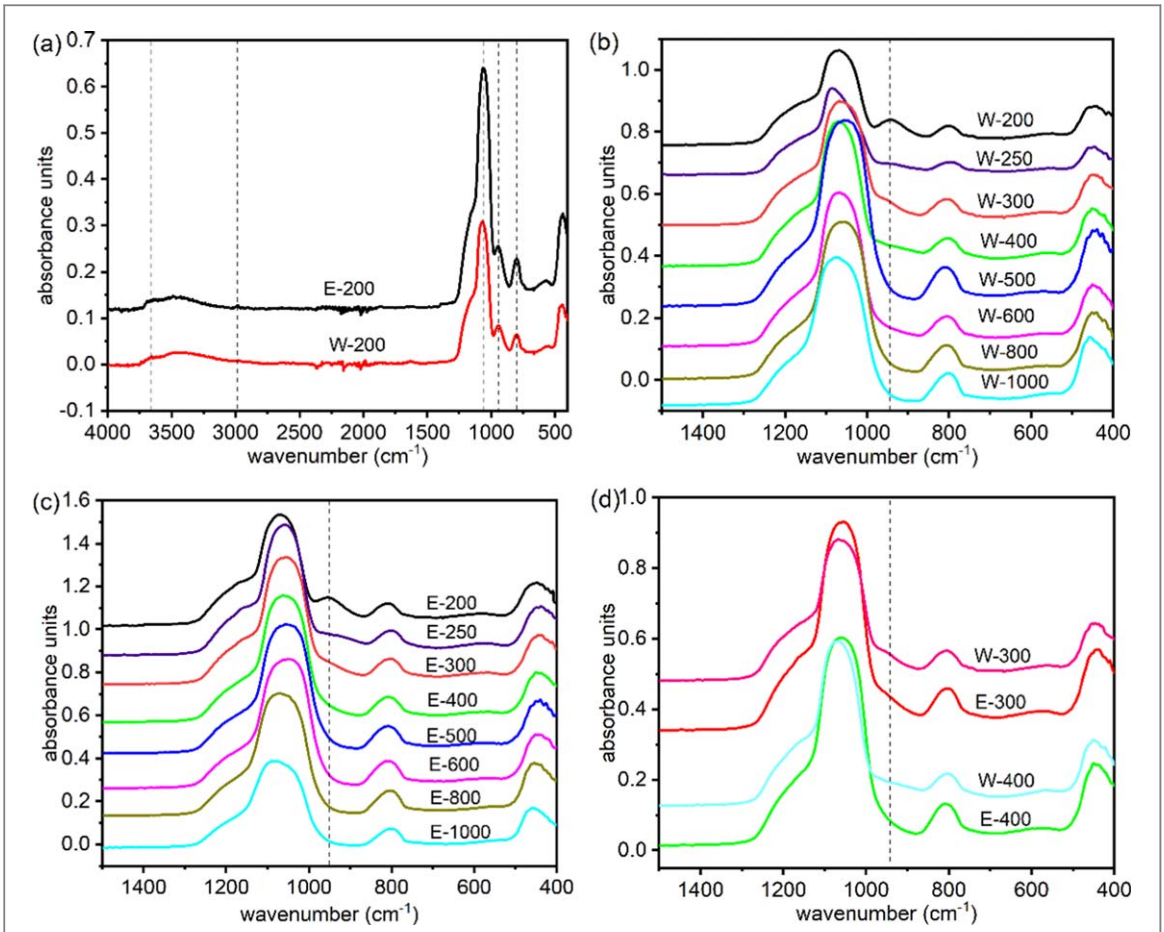

Figure 5. ATR-FTIR spectra of (a) samples W-200 and E-200; (b) the samples washed with water (1500–400 cm^{-1}); (c) the samples washed with ethanol (1500–400 cm^{-1}); (d) samples W-300, W-400, E-300, and E-400 (1500–400 cm^{-1}).

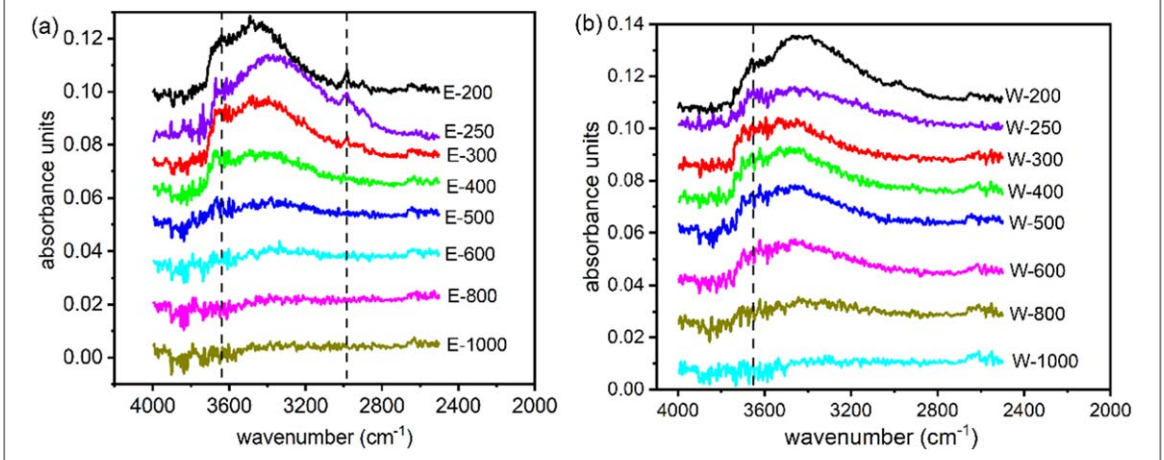

Figure 6. ATR-FTIR spectra (4000–2500 cm^{-1}) of the samples washed with (a) ethanol and (b) water. The dashed lines at over 3600 cm^{-1} in (a) and (b) represent internal silanol, while the dashed line at 2983 cm^{-1} in (a) indicates the peak of C–H bond.

3.4. Calculation

In the literature, the TG mass loss and S_{BET} values have often been used to estimate the surface hydroxyl density of Stöber silica, and the results have yielded a wide range of values (from about 5.7 to 56 OH/nm^2) [25, 45]. The low S_{BET} and the sophisticated internal structure of Stöber silica could be the main reasons behind such discrepant results. In this work, we calculated the specific surface area of sample W-200 using the TG mass loss result (from 200 °C to 1200 °C) and the commonly adopted value of the surface hydroxyl density (4.6 OH nm^{-2}) [41]. During the TG measurements, the sample was first held at 200 °C for 2 h to remove the adsorbed water and

then heated to 1200 °C. For comparison, sample W-200 was mixed with deionized water and vibrated for 24 h to fully hydroxylate the sample surface, while the mass loss in the temperature range from 200 °C to 1200 °C was very close to that of sample W-200 (4.60%), which means the number of hydroxyl groups did not increase during the 24 h of contact with water.

The specific surface area was estimated according to the following equation:

$$S_{cal}(m^2/g) = \frac{\frac{M}{100} \times N_A \times 2}{MW_{H_2O} \times n_{OH} \times 10^{18}} \quad (1)$$

where MW_{H_2O} is the molecular weight of water, N_A is Avogadro's constant, M is the mass loss (%) from 200 °C to 1200 °C, and n_{OH} is the surface silanol density (4.6 OH nm^{-2}). The calculated specific surface area (S_{cal}) is 669.2 $m^2\ g^{-1}$, which is nearly twice the S_{BET} (343.5 $m^2\ g^{-1}$) obtained from the N_2 adsorption measurements. There probably exist narrow pores (<0.8 nm) and even closed pores in the sample, which hinder the motion of nitrogen molecules. Nevertheless, the surface silanols located at narrow (<0.8 nm) and closed pores can be removed during the TG measurements. This may be what caused the S_{cal} to be so large. According to equation (1), we can also use our measured S_{BET} (343.5 $m^2\ g^{-1}$) and TG mass loss (4.60%) to calculate the surface silanol density, which is much higher (8.96 OH nm^{-2}) than 4.6 OH nm^{-2}. In Zhuravlev's measurements, narrow pores (<1 nm) were not considered [41]; thus, the average silanol density of 4.6 OH nm^{-2} may not be suitable for samples with narrow pores when calculating the specific surface area using the TG mass loss and S_{BET}.

4. Conclusion

In order to achieve an improved understanding of the effects of heat treatment on the microporous structure and surface properties of Stöber silica, a series of Stöber silica samples calcined at different temperature were prepared and systematically characterized. For the water-washed sample, the smaller-size micropores (0.8 nm) are the first to collapse or be blocked during calcination. After calcination at 400 °C, the micropores shrink so that the nitrogen molecules cannot enter or diffuse smoothly within the pores. During calcination at 500 °C, the micropores collapse completely. For the ethanol-washed sample, the ethoxyl groups occupy most of the sample surface. After calcination at 500 °C, the ethoxyl groups are completely removed, which can be associated with the collapse of the micropores and agrees with the measured carbon contents. We believe that micropores still exist in the ethanol-washed samples despite the small S_{BET} obtained via N_2 adsorption measurements, but they are blocked by monomers or oligomers and ethoxyl groups. Thus, the variation in the number of micropores is consistent with that of the ethoxyl groups during calcination because most ethoxyl groups are located on the internal pore surface. There is a huge discrepancy between the S_{cal} and the S_{BET} obtained from the N_2 adsorption measurements as well as between the calculated surface silanol density and the commonly adopted value, which illustrates the complexity and extraordinary properties of Stöber silica. After calcination at 800 °C, the significant decrease in TG mass loss indicates nearly complete condensation of surface hydroxyl groups to form siloxane. Our work helps gaining a deeper understanding of the microporous structure and surface groups of Stöber silica as well as their evolution with heating processes. Consequently, our research findings will also facilitate future applications of Stöber silica or Stöber process in a variety of fields.

Acknowledgments

This work was financially supported by Guizhou Provincial Basic Research Program (Natural Science) (QKHJC [2020] 1Y171), the National Natural Science Foundation of China (42163010), and the Academic New Seedling Fund Project of Guizhou Normal University (Qian Shi Xin Miao [2022] No. 26).

Data availability statement

All data that support the findings of this study are included within the article (and any supplementary files).

Competing interests

The authors declare no competing interests.

ORCID iDs

Shanshan Li https://orcid.org/0009-0002-0270-9905

References

[1] Zheng K, Sui B, Ilyasa K and Boccaccini A R 2021 Porous bioactive glass micro- and nanospheres with controlled morphology: developments, properties and emerging biomedical applications *Materials Horizons* **8** 300–35

[2] Maity A and Polshettiwar V 2017 Dendritic fibrous nanosilica for catalysis, energy harvesting, carbon dioxide mitigation, drug delivery, and sensing *Chem. Sus. Chem.* **10** 3866–913

[3] Li H, Chen X P, Shen D Q, Wu F, Pleixats R and Pan J M 2021 Functionalized silica nanoparticles: classification, synthetic approaches and recent advances in adsorption applications *Nanoscale* **13** 15998–6016

[4] Maity A, Belgamwar R and Polshettiwar V 2019 Facile synthesis to tune size, textural properties and fiber density of dendritic fibrous nanosilica for applications in catalysis and CO_2 capture *Nat. Protoc.* **14** 2177–204

[5] Eurov D A, Kurdyukov D A, Medvedev A V, Kirilenko D A, Tomkovich M V and Golubev V G 2021 Micro-mesoporous submicron silica particles with pore size tunable in a wide range: synthesis, properties and prospects for LED manufacturing *Nanotechnology* **32** 215604

[6] Cho S-H, Park S Y, Kim C, Choi P-P and Park J-K 2014 Stabilization of monodispersed spherical silica particles and their alignment with reduced crack density *Colloids and Surfaces a-Physicochemical and Engineering Aspects* **441** 354–9

[7] Husain H, Hariyanto B, Sulthonul M, Klysubun W, Darminto D and Pratapa S 2019 Structure and magnetic properties of silica-coated magnetite-nanoparticle composites *Mater. Res. Express* **6** 086117

[8] Yang D-L, Xiao J, Wang D, Lin W-M and Pu Y 2018 Controllable preparation of monodisperse silica nanoparticles using internal circulation rotating packed bed for dental restorative composite resin *Ind. Eng. Chem. Res.* **57** 12809–15

[9] Yang M H, Wu H H, Wu H Y, Huang C J, Weng W Z, Chen M S and Wan H L 2016 Preparation and characterization of a highly dispersed and stable Ni catalyst with a microporous nanosilica support *RSC Adv.* **6** 81237–44

[10] van der Hoeven J E S, Gurunarayanan H, Bransen M, de Winter D A M, de Jongh P E and van Blaaderen A 2022 Silica-coated gold nanorod supraparticles: a tunable platform for surface enhanced raman spectroscopy *Adv. Funct. Mater.* **32** 2200148

[11] Alessi A, Agnello S, Iovino G, Buscarino G, Melodia E G, Cannas M and Gelardi F M 2014 Thermally induced structural modifications and O_2 trapping in highly porous silica nanoparticles *Mater. Chem. Phys.* **148** 956–63

[12] Koseki K, Arita T, Tabata K, Nohara T and Masuhara A 2021 Effect of surface silanol density on the proton conductivity of polymer-surface-functionalized silica nanoparticles *ACS Sustainable Chemistry & Engineering* **9** 10093–9

[13] Bippus L, Jaber M, Lebeau B, Schleich D and Scudeller Y 2014 Thermal conductivity of heat treated mesoporous silica particles *Microporous Mesoporous Mater.* **190** 109–16

[14] Stöber W, Fink A and Bohn E 1968 Controlled growth of monodisperse silica spheres in the micron size range *J. Colloid Interface Sci.* **26** 62–9

[15] Bogush G H, Tracy M A and Zukoski C F 1988 Preparation of monodisperse silica particles control of size and mass fraction *J. Non-Cryst. Solids* **104** 95–106

[16] Wang X-D, Shen Z-X, Sang T, Cheng X-B, Li M-F, Chen L-Y and Wang Z-S 2010 Preparation of spherical silica particles by stöber process with high concentration of tetra-ethyl-orthosilicate *J. Colloid Interface Sci.* **341** 23–9

[17] Carcouët C *et al* 2014 Nucleation and growth of monodisperse silica nanoparticles *Nano Lett.* **14** 1433–8

[18] Huang Y and Pemberton J E 2010 Synthesis of uniform, spherical sub-100nm silica particles using a conceptual modification of the classic LaMer model *Colloids Surf.* A **360** 175–83

[19] Daneshfar Z, Goharpey F and Yeganeh J K 2018 Preparation and characterization of modified SiO_2 nanospheres with dichlorodimethylsilane and phenyltrimethoxysilane *Mater. Res. Express* **5** 095005

[20] Lei X, Yu B, Cong H-L, Tian C, Wang Y-Z, Wang Q-B and Liu C-K 2014 Synthesis of monodisperse silica microspheres by a modified Stöber method *Integr. Ferroelectr.* **154** 142–6

[21] Li J, Chen L, Zhang Z and Jiao C 2014 Facile and controlled synthesis of silica sol nanospheres through a modified sol-gel process *Journal of Wuhan University of Technology-Materials Science Edition* **29** 478–82

[22] Kobayashi M, Skarba M, Galletto P, Cakara D and Borkovec M 2005 Effects of heat treatment on the aggregation and charging of Stöber -type silica *J. Colloid Interface Sci.* **292** 139–47

[23] Romeis S, Paul J, Hanisch M, Marthala V R R, Hartmann M, Taylor R N K, Schmidt J and Peukert W 2014 Correlation of enhanced strength and internal structure for heat-treated submicron stöber silica particles *Part. Part. Syst. Charact.* **31** 664–74

[24] Topuz B, Simsek D and Ciftcioglu M 2015 Preparation of monodisperse silica spheres and determination of their densification behaviour *Ceram. Int.* **41** 43–52

[25] Kim J M, Chang S M, Kong S M, Kim K S, Kim J and Kim W S 2009 Control of hydroxyl group content in silica particle synthesized by the sol-precipitation process *Ceram. Int.* **35** 1015–9

[26] Szekeres M, Toth J and Dekany I 2002 Specific surface area of Stöber silica determined by various experimental methods *Langmuir* **18** 2678–85

[27] Dékány I, Németh J, Szekeres M and Schoonheydt R 2003 Surfacial, liquid sorption and monolayer-forming properties of hydrophilic and hydrophobic Stöber silica particles *Colloid. Polym. Sci.* **282** 1–6

[28] Wan Q, Ramsey C and Baran G 2010 Thermal pretreatment of silica composite filler materials *J. Therm. Anal. Calorim.* **99** 237–43

[29] Wells J D, Koopal L K and Keizer A d 2000 Monodisperse, nonporous, spherical silica particles *Colloids Surf.* A **166** 171–6

[30] Labrosse A and Burneau A 1997 Characterization of porosity of ammonia catalysed alkoxysilane silica *J. Non-Cryst. Solids* **221** 107–24

[31] Parnell S R, Washington A L, Parnell A J, Walsh A, Dalgliesh R M, Li F, Hamilton W A, Prevost S, Fairclough J P and Pynn R 2016 Porosity of silica Stöber particles determined by spin-echo small angle neutron scattering *Soft Matter* **12** 4709–14

[32] Balas F, Rodriguez-Delgado M, Otero-Arean C, Conde F, Matesanz E, Esquivias L, Ramirez-Castellanos J, Gonzalez-Calbet J and Vallet-Regi M 2007 Structural characterization of nanosized silica spheres *Solid State Sci.* **9** 351–6

[33] Howard A and Khdary N 2007 Spray synthesis of monodisperse sub-micron spherical silica particles *Mater. Lett.* **61** 1951–4

[34] Davis P J, Deshpande R, Smith D M, Brinker C J and Assink R A 1994 Pore structure evolution in silica gel during aging/drying: IV. Varying pore fluid pH *J. Non-Cryst. Solids* **167** 295–306

[35] Filipović R, Obrenović Z, Stijepović I, Nikolić L M and Srdić V V 2009 Synthesis of mesoporous silica particles with controlled pore structure *Ceram. Int.* **35** 3347–53

[36] Li S, Wan Q, Qin Z, Fu Y and Gu Y 2015 Understanding Stöber silica's pore characteristics measured by gas adsorption *Langmuir* **31** 824–32
[37] Li S, Wan Q, Qin Z, Fu Y and Gu Y 2016 Unraveling the mystery of Stöber silica's microporosity *Langmuir* **32** 9180–7
[38] Thommes M, Kaneko K, Neimark A V, Olivier J P, Rodriguez-Reinoso F, Rouquerol J and Sing K S W 2015 Physisorption of gases, with special reference to the evaluation of surface area and pore size distribution (IUPAC Technical Report) *Pure Appl. Chem.* **87** 1051–69
[39] Reichenbach C, Enke D, Moellmer J, Klank D, Klauck M and Kalies G 2013 Slow gas uptake and low pressure hysteresis on nanoporous glasses: the influence of equilibration time and particle size *Microporous Mesoporous Mater.* **181** 68–73
[40] Li S, Wan Q, Qin Z, Fu Y and Gu Y 2019 Stöber silica's microporosity: insights from thermal analysis studies *J. Therm. Anal. Calorim.* **136** 1895–904
[41] Zhuravlev L T 2000 The surface chemistry of amorphous silica. Zhuravlev model *Colloids and Surfaces a-Physicochemical and Engineering Aspects* **173** 1–38
[42] Ding Y D, Chu X Y, Hong X, Zou P and Liu Y C 2012 The infrared fingerprint signals of silica nanoparticles and its application in immunoassay *Appl. Phys. Lett.* **100** 013701
[43] Primeau N, Vautey C and Langlet M 1997 The effect of thermal annealing on aerosol-gel deposited SiO_2 films: a FTIR deconvolution study *Thin Solid Films* **310** 47–56
[44] Gallas J P, Lavalley J C, Burneau A and Barres O 1991 Comparative-study of the surface hydroxyl-groups of fumed and precipitated silicas. 4. Infrared study of dehydroxylation by thermal treatments *Langmuir* **7** 1235–40
[45] Mueller R, Kammler H K, Wegner K and Pratsinis S E 2003 OH surface density of SiO_2 and TiO_2 by thermogravimetric analysis *Langmuir* **19** 160–5